

REPORT DOCUMENTATION PAGE*Form Approved
OMB No. 0704-0188*

The public reporting burden for this collection of information is estimated to average 1 hour per response, including the time for reviewing instructions, searching existing data sources, gathering and maintaining the data needed, and completing and reviewing the collection of information. Send comments regarding this burden estimate or any other aspect of this collection of information, including suggestions for reducing the burden, to the Department of Defense, Executive Services and Communications Directorate (0704-0188). Respondents should be aware that notwithstanding any other provision of law, no person shall be subject to any penalty for failing to comply with a collection of information if it does not display a currently valid OMB control number.

PLEASE DO NOT RETURN YOUR FORM TO THE ABOVE ORGANIZATION.

1. REPORT DATE (DD-MM-YYYY)		2. REPORT TYPE		3. DATES COVERED (From - To)	
4. TITLE AND SUBTITLE			5a. CONTRACT NUMBER		
			5b. GRANT NUMBER		
			5c. PROGRAM ELEMENT NUMBER		
6. AUTHOR(S)			5d. PROJECT NUMBER		
			5e. TASK NUMBER		
			5f. WORK UNIT NUMBER		
7. PERFORMING ORGANIZATION NAME(S) AND ADDRESS(ES)				8. PERFORMING ORGANIZATION REPORT NUMBER	
9. SPONSORING/MONITORING AGENCY NAME(S) AND ADDRESS(ES)				10. SPONSOR/MONITOR'S ACRONYM(S)	
				11. SPONSOR/MONITOR'S REPORT NUMBER(S)	
12. DISTRIBUTION/AVAILABILITY STATEMENT					
13. SUPPLEMENTARY NOTES					
14. ABSTRACT					
15. SUBJECT TERMS					
16. SECURITY CLASSIFICATION OF:			17. LIMITATION OF ABSTRACT	18. NUMBER OF PAGES	19a. NAME OF RESPONSIBLE PERSON
a. REPORT	b. ABSTRACT	c. THIS PAGE			19b. TELEPHONE NUMBER (Include area code)

15-1231-1161

PUBLICATION OR PRESENTATION RELEASE REQUEST

Publity 811

NRL 5510.40

Ref: (a) NRL Instruction 5600.2 (b) NRL Instruction 5510.40E	<input type="checkbox"/> Abstract only, published <input type="checkbox"/> Book author <input type="checkbox"/> Book editor <input type="checkbox"/> Conference Proceedings (refereed) <input checked="" type="checkbox"/> Journal article (refereed) <input type="checkbox"/> Oral Presentation, published <input type="checkbox"/> Video <input type="checkbox"/> Poster	<input type="checkbox"/> Abstract only, not published <input type="checkbox"/> Book chapter <input type="checkbox"/> Multimedia report <input type="checkbox"/> Conference Proceedings (not refereed) <input type="checkbox"/> Journal article (not refereed) <input type="checkbox"/> Oral Presentation, not published <input type="checkbox"/> Other, explain	STRN <u>NRL/JA/7330-15-2528</u> Route Sheet No. <u>7330/</u> Job Order No. <u>73-4951-05-5</u> ✓ Classification <u>U</u> <u>S</u> <u>C</u> FOUO Sponsor <u>ONR BASE</u> <u>601-Bje</u> Sponsor's approval <u>yes*</u> (attached) (*Required if research is other than 6.1/6.2 NRL or ONR unclassified research or if publication/presentation is classified)
---	--	---	---

ALL DOCUMENTS/PRESENTATIONS MUST BE ATTACHE

Title of Paper or Presentation
A fast-response fiber-optic anemometer with temperature self-compensation

AUTHOR(S) LEGAL NAMES(S) OF RECORD (First, MI, Last), CODE, (Affiliation if not NRL).
Guigen Liu University of Nebraska-Lincoln, Weilin Hou 7333, Wei Qiao University of Nebraska-Lincoln, Ming Han University of Nebraska-Lincoln

This paper will be presented at the Optics Express
(Name of Conference)

(Date, Place and Classification of Conference)

and/or for published in Optics Express, Unclassified
(Name and Classification of Publication)

(Name of Publisher)

It is my opinion that the subject paper (is) (is not X) classified, in accordance with reference (b) and this paper does not violate any disclosure of trade secrets or suggestions of outside individuals or concerns which have been communicated to the NRL in confidence.

This subject paper (has) (has never X) been incorporated in an official NRL Report.

Weilin Hou, 7333
Name and Code (Principal Author) (Legal Name of Record and Signature Only) [Signature] (Signature)

APPROVAL NOTE: If name other than your own is entered on the publication or presentation itself, add an explanatory note in the caption below next to your signed legal name of

CODE	SIGNATURE	DATE	COMMENTS
Co-Author(s) Weilin Hou, 7333	<u>[Signature]</u>	<u>3/27/15</u>	Need by <u>17 Apr 2015</u>
Section Head	<u>[Signature]</u>	<u>3/27/15</u>	This is a Final Security Review. Any changes made in the document, after approved by Code 1231, nullify the Security Review.
Branch Head Richard L. Crout, 7330	<u>[Signature]</u>	<u>3/27/2015</u>	
Division Head	<u>[Signature]</u>	<u>3/30/15</u>	1. To the best knowledge of this Division, the subject matter of this publication (has <u> </u>) (has never <u> X </u>) been classified. 2. This paper (does <u> </u>) (does not <u> X </u>); contain any militarily critical technology.
Ruih H. Preller, 7300	<u>[Signature]</u>	<u>3/30/15</u>	
ADDR/Director NCST E. R. Franchi, 7000	<u>[Signature]</u>	<u>4/9/15</u>	A copy of the paper, abstract or presentation is filed in this office.
SEC/CO	<u>[Signature]</u>	<u>5-8-2015</u>	
Security, Code 1231	<u>[Signature]</u>	<u>4-17-15</u>	
Associate Counsel, Code 1008.3	<u>[Signature]</u>	<u>4-17-15</u>	
Public Affairs (Unclassified/ Unlimited Only), Code 7030.4	<u>[Signature]</u>	<u>4-17-15</u>	
Division, Code			
Author, Code			

[Large Handwritten Mark]

Fast-response fiber-optic anemometer with temperature self-compensation

Guigen Liu,¹ Weilin Hou,² Wei Qiao,¹ and Ming Han^{1,*}

¹Department of Electrical and Computer Engineering, University of Nebraska-Lincoln, Lincoln, NE 68588, USA

²Naval Research Laboratory, Code 7333, Stennis Space Center, MS 39529, USA

*mhan@unl.edu

Abstract: We report a novel fiber-optic anemometer with self-temperature compensation capability based on a Fabry-Pérot interferometer (FPI) formed by a thin silicon film attached to the end face of a single-mode fiber. Guided in the fiber are a visible laser beam from a 635 nm diode laser used to heat the FPI and a white-light in the infrared wavelength range as the signal light to interrogate the optical length of the FPI. Cooling effects on the heated sensor head by wind is converted to a wavelength blueshift of the reflection spectral fringes of the FPI. Self-temperature-compensated measurement of wind speed is achieved by recording the difference in fringe wavelengths when the heating laser is turned on and then off. Large thermal-optic coefficient and thermal expansion coefficient of silicon render a high sensitivity that can also be easily tuned by altering the heating laser power. Furthermore, the large thermal diffusivity and the small mass of the thin silicon film endow a fast sensor response.

©2015 Optical Society of America

OCIS codes: (060.2370) Fiber optics sensors; (120.6810) Thermal effects; (120.2230) Fabry-Perot ; (120.3180) Interferometry.

References and links

1. R. Chen, A. Yan, Q. Wang, and K. P. Chen, "Fiber-optic flow sensors for high-temperature environment operation up to 800°C," *Opt. Lett.* **39**(13), 3966–3969 (2014).
2. C. Jewart, B. McMillen, S. K. Cho, and K. P. Chen, "X-probe flow sensor using self-powered active fiber Bragg gratings," *Sens. Actuators A Phys.* **127**(1), 63–68 (2006).
3. D. W. Lamb and A. Hooper, "Laser-optical fiber Bragg grating anemometer for measuring gas flows: application to measuring the electric wind," *Opt. Lett.* **31**(8), 1035–1037 (2006).
4. O. Frazão, P. Caldas, F. M. Araújo, L. A. Ferreira, and J. L. Santos, "Optical flowmeter using a modal interferometer based on a single nonadiabatic fiber taper," *Opt. Lett.* **32**(14), 1974–1976 (2007).
5. J. Lee and J. Kim, "Elastomeric microwire-based optical gas flowmeter with stretching-enabled tunability in measurement range," *Opt. Lett.* **36**(19), 3789–3791 (2011).
6. S. Takashima, H. Asanuma, and H. Niitsuma, "A water flowmeter using dual fiber Bragg grating sensors and cross-correlation technique," *Sens. Actuators A Phys.* **116**(1), 66–74 (2004).
7. G. D. Byrne, S. W. James, and R. P. Tatam, "A Bragg grating based fibre optic reference beam laser Doppler anemometer," *Meas. Sci. Technol.* **12**, 909–914 (2001).
8. C.-L. Lee, C.-F. Lee, C.-M. Li, T.-C. Chiang, and Y.-L. Hsiao, "Directional anemometer based on an anisotropic flat-clad tapered fiber Michelson interferometer," *Appl. Phys. Lett.* **101**(2), 023502 (2012).
9. S. Gao, A. P. Zhang, H.-Y. Tam, L. H. Cho, and C. Lu, "All-optical fiber anemometer based on laser heated fiber Bragg gratings," *Opt. Express* **19**(11), 10124–10130 (2011).
10. T. Chen, Q. Wang, B. Zhang, R. Chen, and K. P. Chen, "Distributed flow sensing using optical hot-wire grid," *Opt. Express* **20**(8), 8240–8249 (2012).
11. S. Takagi, "A hot-wire anemometer compensated for ambient temperature variations," *J. Phys. E Sci. Instrum.* **19**(9), 739–743 (1986).
12. G. Liu, M. Han, and W. Hou, "High-resolution and fast-response fiber-optic temperature sensor using silicon Fabry-Pérot cavity," *Opt. Express* **23**(6), 7237–7247 (2015).
13. M. N. Özisik, *Heat Transfer: A Basic Approach* (McGraw-Hill, 1985).
14. M. A. Green, "Self-consistent optical parameters of intrinsic silicon at 300 K including temperature coefficients," *Sol. Energy Mater. Sol. Cells* **92**(11), 1305–1310 (2008).

1. Introduction

Measurement of speed of gas or liquid flow is of great practical importance in a variety of industries, such as pharmacy, oil exploration, chemical plants, and oceanography research. Owing to their many unique advantages, such as small size, light weight, immunity to electromagnetic interference, and remote sensing capability in harsh environments, fiber-optic flowmeters or anemometers have proven to be attractive alternatives to their traditional mechanical or electromagnetic counterparts and have been extensively studied in the past few years [1–6].

The sensing mechanism of a fiber-optic flowmeter or anemometer varies significantly from one to another. For example, a fiber Bragg grating (FBG) anemometer based on Doppler effects has been reported [7]. An anisotropic flat-clad tapered fiber Michelson interferometer has been devised to report both wind direction and wind speed by interrogating the bending of the fiber in response to wind [8]. A few other fiber-optic anemometers are based on the bending of a tapered single-mode fiber (SMF) [4] or an elastic poly microwire [5]. Hot-wire based fiber-optic anemometers are another type that has been widely investigated and have shown great promise [1–3, 9, 10]. In particular, the laser heated fiber-optic hot-wire anemometers exhibit controllable sensitivity, responsibility and dynamic range. The principle of hot-wire anemometers is that the cooling effect brought by wind reduces the temperature of the sensor, which in turn causes a signal change such as a shift of the FBG wavelength. In addition to the cooling by wind, the wind temperature itself also influences the readouts of the anemometer. The elimination of the cross-sensitivity to wind temperature is therefore a key and inevitable issue of the hot-wire anemometers. While methods for temperature compensation in electronic hot-wire anemometers have been investigated [11], few efforts have been devoted to temperature-compensation of fiber-optic anemometers. According to the theoretical model for a FBG hot-wire anemometer [9], the heat loss is related to the product of the temperature difference and the square root of wind speed. Therefore, it is a fundamental challenge to distinguish the signals from the wind temperature and those from wind speed, even with the help of a separate reference temperature sensor.

In this paper, taking advantage of the unique optical and thermal properties of silicon material, we demonstrate a miniature fiber-optic anemometer based on a silicon Fabry-Pérot interferometer (FPI) formed at the tip of a SMF that possesses many advantages over previously reported sensors. We show that the sensor, heated by a visible laser and interrogated by a broadband infrared (IR) light, has the ability to distinguish the signal induced by wind temperature and that by wind speed through controlling heating laser power and observing the fringe shifts from the cooling effect of wind speed. The proposed sensor also possesses high sensitivity and fast response due to the large thermal diffusivity, large thermo-optic coefficient (TOC), and large thermal expansion coefficient (TEC) of silicon.

The rest of the paper is arranged as follows: sensor structure, principle of operation, and comprehensive theoretical analysis are provided in Section 2; followed by the experimental demonstration in Section 3; and the final conclusion is presented in Section 4.

2. Principle of operation and theoretical analysis

The structure of the fiber-optic anemometer is schematically shown in Fig. 1(a). A 10 μm -thick silicon film is mounted on the endface of a SMF forming an FPI that gives rise to fringes in the reflection spectrum. The signal white-light centered at 1550 nm is injected through the SMF to the FPI and the reflection spectrum is recorded by a high-speed spectrometer. At the same time, a heating light from a 635 nm diode laser is guided through the same SMF to the heat the FPI. Silicon has a band gap energy of 1.11 eV and highly transparent to signal light but is opaque to the heating laser. Therefore the FPI temperature can be effectively increased by the laser heating. When the wind blows over the surface of hot silicon film, cooling effects will reduce the temperature of the silicon FPI and introduce a

blue shift to the fringe valley wavelength of the reflection spectrum, as schematically shown in Fig. 1(b). As theoretically shown below and experimentally demonstrated in Section 3, the wavelength shift can be separated into the wind-temperature-induced wavelength shift and the wind-speed-induced wavelength shift. As a result, temperature self-compensated measurement of wind speed is achieved by the difference in the wavelengths of a fringe valley when the heating laser is turned on and off to achieve the temperature-compensated wind speed.

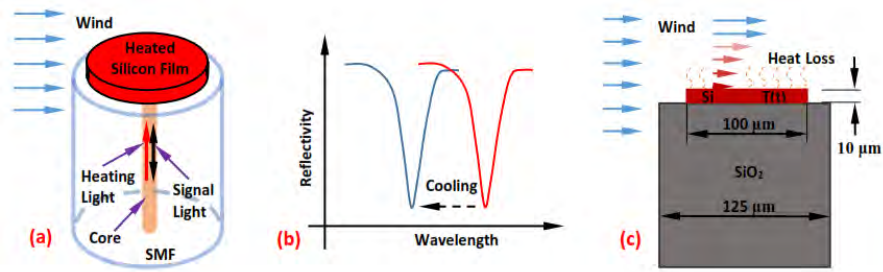


Fig. 1. (a) Schematic illustration of the proposed wind probe. (b) Blueshift of the wavelength dip in response to the cooling effects by blowing wind. (c) Schematic model for the heat transfer analysis.

The wavelength position of the N^{th} fringe valley, λ_N , in the reflection spectrum of the silicon FPI is expressed as

$$N\lambda_N = 2nL, \quad (1)$$

where n and L are, respectively, the RI and cavity length of the silicon FPI. Owing to the thermo-optic effect and thermal expansion, both n and L are functions of the FPI temperature. Therefore, λ_N can be used for measurement of the FPI's temperature and its sensitivity is given by

$$\frac{\partial \lambda_N}{\partial T} = \lambda_N \left(\frac{1}{n} \frac{\partial n}{\partial T} + \frac{1}{L} \frac{\partial L}{\partial T} \right). \quad (2)$$

In Eq. (2), $\partial n / \partial T$ and $\frac{\partial L}{\partial T} / L$ are, respectively, the TOC and TEC of silicon, both of which are assumed to be constants within the temperature range in our experiment (from room temperature to less than 100 °C). Integrating Eq. (2) on both sides and, for simplicity, ignoring the symbol for the fringe order lead to

$$\lambda = \lambda_0 + KT. \quad (3)$$

where λ_0 is the intercept wavelength, $K = \lambda_N \left(\frac{\partial n}{\partial T} / n + \frac{\partial L}{\partial T} / L \right)$ is the temperature sensitivity.

As shown in our previous work [12], the large TOE and TEC of silicon can lead to significantly improved sensitivity and resolution than silica-based fiber-optic temperature sensors.

The existence of heating light increases the temperature of the silicon FPI above that of the ambient air. When the sensor is placed in wind, the temperature of the heated silicon film will decrease due to the loss of heat energy, leading to a blueshift in the fringe valley wavelength as shown in Fig. 1(b). To facilitate the quantitative evaluation of the temperature variation in response to the wind speed, a model for heat transfer analysis is constructed, as

schematically shown in Fig. 1(c). In this model, due to the much larger horizontal dimension than its thickness, the silicon film is regarded as a flat hot plate with heat losses on the top surface over which the wind blows. The silica fiber is considered as an adiabatic base in the transient heat analysis because thermal conductivity of silicon ($\sim 159 \text{ W/m/K}$ at 25°C) is more than two orders of magnitude larger than that of silica ($\sim 1.3 \text{ W/m/K}$) at 25°C . The heat transfer from the sensor to the environment can be divided into two processes. The first process is the heat transfer from the silicon film to the wind and the second one is heat dissipation within the silicon film. The speed of thermal energy exchange during the first process is quantified by the heat transfer coefficient (HTC), h ; while the speed of the thermal conduction within the silicon film (the second process) is quantified by the thermal conductivity of silicon, K_s . To compare the speed of these two processes, the well-known dimensionless Biot number is calculated as [13]

$$B_i = \frac{h \cdot L_c}{K_s}, \quad (4)$$

where L_c is the characteristic length of the silicon film. To calculate h , the average Nusselt number N_u for forced convection (laminar flow) over a flat plate is calculated first according to [13],

$$N_u = 0.664 \text{Pr}^{1/3} \text{Re}_L^{1/2} \quad (0.6 < \text{Pr} < 10, \text{Re}_L < 5 \times 10^5), \quad (5)$$

where $\text{Pr} = \nu / \alpha$ is the Prandtl number and $\text{Re}_L = uL_c / \nu$ is the Reynolds number. The parameters of ν , α , and u are, respectively, the kinematic viscosity, the thermal diffusivity and the speed of wind (air). Note that Eq. (5) for calculating the averaged Nusselt number of the air blowing over the flat silicon film is valid only for the wind speed that is not too low. Otherwise, the Nusselt number derived for natural convection should be applied instead. Once N_u is obtained, $h = N_u K_w / L_c$ can be calculated, where K_w is the thermal conductivity of wind (air). Using the following parameters [13], $\nu = 1.6 \times 10^{-5} \text{ m}^2 / \text{s}$, $\alpha = 2.295 \times 10^{-5} \text{ m}^2 / \text{s}$, $u = 2.295 \times 10^{-5} \text{ m}^2 / \text{s}$, $L_c = 100 \mu\text{m}$, $K_w = 0.0257 \text{ W} / (\text{m} \cdot \text{K})$, it is calculated that $B_i = 4.78 \times 10^{-4}$. Since $B_i \ll 1$, the speed of heat conduction within the silicon film is much faster than the heat exchange between wind and silicon. In this situation, the lumped system analysis (LSA) can be used for heat transfer analysis with a negligible error (less than about 5 percent for $B_i < 0.1$) [13]. The LSA suggests that the temperature distribution within the silicon thin film at any instant is sufficiently uniform that the temperature of the silicon thin film can be considered to be a function of time only. With a heating source within the sensor, the model for LSA is expressed as [13],

$$hA_s [T_w - T(t)] dt + P dt = \rho_s C_s V_s dT(t), \quad (6)$$

where A_s is the surface area for heat exchange, T_w is the wind temperature, P is the heating power within the silicon wafer, ρ_s , C_s , and V_s are, respectively, the density, the thermal capacity, and the volume of the silicon film. Solution to Eq. (6) is given by

$$T(t) = T_w + \frac{P}{hA_s} + \left(T_0 - T_w - \frac{P}{hA_s} \right) \exp\left(-\frac{hA_s}{\rho_s C_s V_s} t \right), \quad (7)$$

where T_0 is the initial temperature of the sensor. Obviously, the right hand side (RHS) of Eq. (7) can be separated into two parts, the first part $T_\infty = T_w + P / (hA_s)$ represents the steady-state temperature (SST) and the rest represents the transient part which determines the speed of the sensor response. It can be seen that the SST consists of two terms: the first one is the wind temperature (T_w) and the second one is the temperature increment ($P / (hA_s)$) due to the combined effects of heating laser power and wind speed. It is seen that the temperature change caused by wind speed is separated from the wind temperature. To obtain the temperature increment in experiment, the SSTs with heating power off ($P = 0$) and on ($P > 0$) are measured consecutively and the difference between these two SSTs is a function of the wind speed only. The coefficient, $hA_s / (\rho_s C_s V_s)$, in the exponent of the transient term in RHS of Eq. (7) characterizes the response time of the anemometer.

Conversion of the temperature into fringe valley wavelength is accomplished by substituting Eq. (7) into Eq. (3), which gives rise to

$$\begin{aligned} \lambda(t) &= \lambda_0 + KT(t) \\ &= \lambda_0 + KT_w + K \frac{P}{hA_s} + K \left(T_0 - T_w - \frac{P}{hA_s} \right) \exp \left(- \frac{hA_s}{\rho_s C_s V_s} t \right), \end{aligned} \quad (8)$$

Substituting the expression for h ($h = N_u K_w / L_c$) and using Eq. (5), the wavelength shift caused by wind speed u at the steady state can be derived as

$$\Delta\lambda = K \frac{P}{hA_s} = \frac{1.5KL_c^{1/2} v^{1/6} \alpha^{1/3}}{K_w A_s} \frac{P}{u^{1/2}}. \quad (9)$$

Equation (9) suggests that the wavelength shift is linearly proportional to the heating laser power P , but inversely proportional to the square root of the wind speed u . The transient term of Eq. (8) gives the response time, τ , as

$$\tau = \frac{\rho_s C_s V_s}{hA_s} = \frac{1.5L_c^{1/2} v^{1/6} \alpha^{1/3} \rho_s C_s V_s}{K_w A_s} \frac{1}{u^{1/2}} \quad (10)$$

It is seen that the response time can be reduced by using a small sensing element, e.g., a thinner (smaller L_c) silicon film with a large surface-to-volume ratio (A_s / V_s). In addition, the response time is also dependent on the wind speed and the sensor responds faster to larger wind speed. These are expected as both smaller sensing element and higher wind speed facilitate the heat exchange between sensing element and surrounding, leading to the faster response.

3. Experimental demonstration

The sensor fabrication followed similar procedures as reported in detail in our previous work [12]. Here, the double-side-polished silicon film has the shape of thin cylinder with a thickness of 10 μm and diameter of around 100 μm . A microscope picture of the sensor head is shown in the inset to Fig. 2(a). As the anemometer relies on the measurement of the wavelength shift in response to temperature change brought by the wind, we first investigated the temperature sensitivity of the sensor. Figure 2(a) shows the reflection spectra of the silicon FPI at different temperatures. Clearly, the spectral fringes shift toward longer wavelength as temperature increases. The fringe valley wavelength as a function of temperature and its linear fit are shown in Fig. 2(b), indicating a temperature sensitivity of ~ 84.5 pm/ $^\circ\text{C}$.

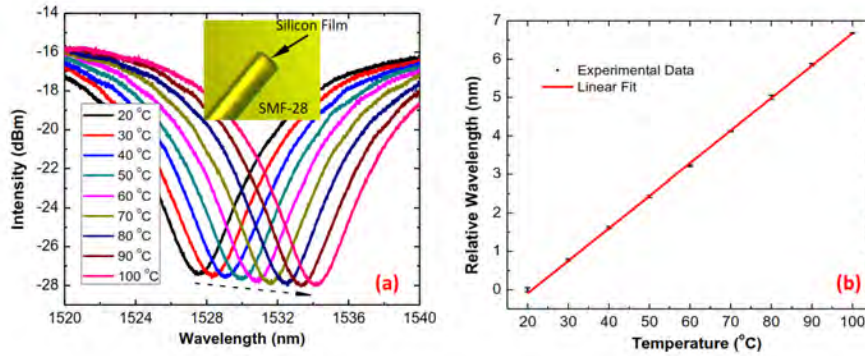


Fig. 2. (a) Reflection spectra at different temperatures. Inset shows the fiber probe. (b) Relative dip wavelength with respect to temperature.

The wind speed measurement by the anemometer is demonstrated using a setup schematically shown in Fig. 3(a). A broadband source with an output power of 12 mW (Ibsen Photonics, DL-BP1 1501A) provided signal light for the FPI via a circulator, and the reflected signal light was acquired by a high-speed spectrometer (Ibsen Photonics, I-MON 256 USB) which was connected to a computer for control and data collection. A 635 nm laser diode (LPS-635-FC, Thorlabs) was used as the heating light source that heated the silicon FPI via a fiber-optic coupler. The sensor tip was taped on one side of the sensing probe of a commercial anemometer (OMEGA, FMA1002R-V1) which served as a reference and calibration of our fiber-optic sensor. The wind speed was controlled by home-made wind tunnel in which the sensor probe was placed.

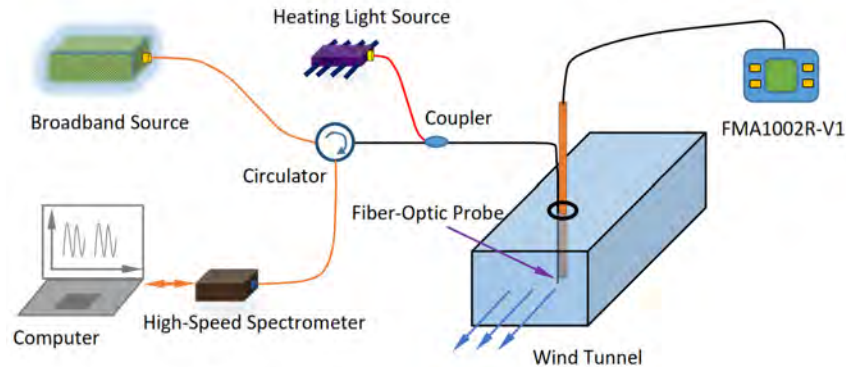


Fig. 3. Schematic of the experimental setup for sensor demonstration and testing.

It is worth pointing out that, while the low absorption loss of silicon in the IR wavelength (1550 nm window here) generates interferometric fringes with good visibility from the silicon FPI, practically no interference can occur at the visible wavelength of 635 nm for the sensor proposed here because of the extremely high absorption of silicon at this wavelength [14]. For example, the absorption depth (defined as the depth where light intensity has fallen to $1/e$ of its original value) at 635 nm is only $3.1 \mu\text{m}$ [14]. After a round trip of the $10\text{-}\mu\text{m}$ long FPI, only 0.0076% of the heating laser power remains (assuming the reflectances at silicon-air and silicon-silica interfaces are, respectively, 29.8% and 16.2%). As a result, it is reasonable to assume that the heating laser power absorbed by the FPI is insensitive to the variations in the optical length of the FPI.

We first characterized the fringe valley wavelength (λ) as function of heating laser power (i.e., P in Eq. (9), in unit of laser current) in different wind speeds (u). Note that, although the pigtail fiber of the heating laser is single mode at the laser wavelength, the pigtail fiber (SMF-28) of the coupler becomes multimode at the wavelength. As a result, the coupling ratio at the heating laser wavelength is sensitive to fiber bending and temperature variations and it is difficult to accurately obtain the heating laser power delivered to the FPI. Therefore, the laser current is used to represent the power of the heating laser. According to the laser specification, the power coupled to the pigtail SMF of the heating laser is ~ 2.5 mW when the laser current is 70 mA with a slope efficiency of ~ 0.18 mW/mA. The results and their linear fits are shown in Fig. 4. The adjusted R^2 values of the linear fits for wind speeds of 2.7, 3.5, and 4 m/s are, respectively, 0.976, 0.979, and 0.970, indicating a good linearity of wavelength in response to the heating laser power that agrees with Eq. (9). The linear fits for wind speeds of 2.7, 3.5, and 4.0 m/s have, respectively, slopes of 0.138, 0.149, and 0.164. According to Eq. (9), the slope of the λ vs. P curve is proportional to $u^{-1/2}$, which is verified by the observation that $0.138/2.7^{1/2} = 0.084$, $0.149/3.5^{1/2} = 0.080$, and $0.164/4.0^{1/2} = 0.082$ are very close to each other. The small discrimination among these values is believed to arise from the weak temperature dependence of the material parameters in Eq. (9).

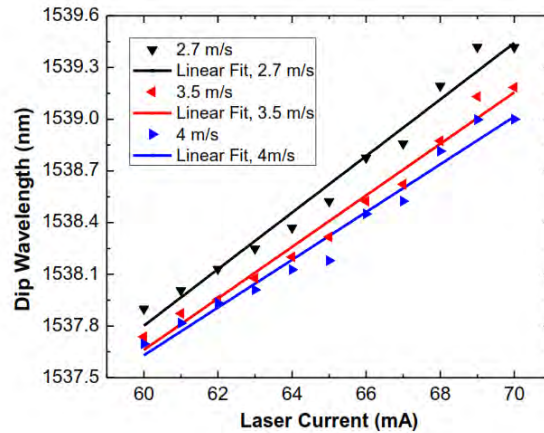


Fig. 4. Fringe valley wavelength with respect to heating laser power at different wind speeds.

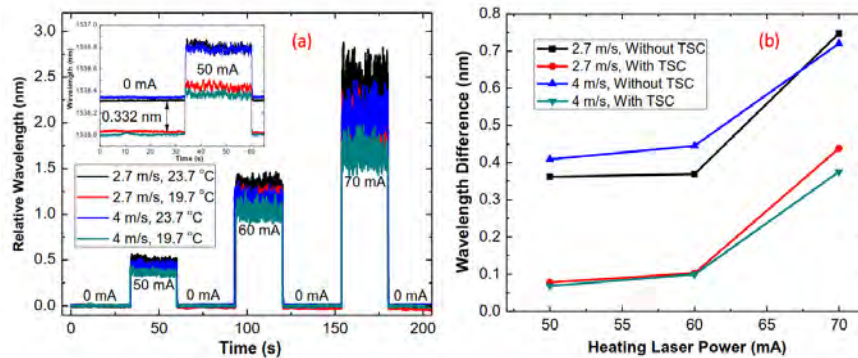


Fig. 5. (a) Relative wavelength at different heating powers when the sensor is placed in wind with temperature of 19.7 °C or 23.7 °C and speed of 2.7 m/s or 4 m/s. Inset exhibits the original curves to show the wavelength difference due to the different wind temperatures, the legend also applies to the inset. (b) Wavelength difference measured for a certain wind speed due to different wind temperatures (19.7 °C and 23.7 °C) with respect to heating laser power.

To examine the capability of temperature self-compensation (TSC), the anemometer was tested in winds with two different temperatures (23.7 °C and 19.7 °C) at a wind speed of 2.7 m/s and 4 m/s. First, the wind tunnel and the sensor system were placed in a room with a temperature of 23.7 °C. For each of the wind speeds, the reflection spectra were acquired at a frame rate of 200 Hz when the heating laser was turned off for ~30 s and then turned on for ~30 s with a current of 50 mA; this process was also repeated for heating laser currents of 60 mA and 70 mA. Then the room temperature was changed to 19.7 °C and the same testing process performed at 23.7 °C was repeated.

The experimental results are shown in Fig. 5. The difference of ~0.332 nm in the initial wavelengths when heating power was turned off, shown in the inset to Fig. 5(a), was due to the 4 °C difference in wind temperature (the slight difference in wavelength for different wind speeds at the supposedly same room temperature is attributed to the fluctuations of the room temperature). Clearly, the wind temperature itself introduces large shifts in wavelength, which has to be compensated for accurate wind speed measurement. As stated in the theoretical analysis, the difference between wavelengths when the heating power is on and off is due to the wind speed only. For the convenience of comparison, the wavelength shift relative to the initial wavelength when the laser was off is shown in Fig. 5(a). It is seen that the wavelength shifted when the heating laser was turned on and returned to the base line when the heating was turned off. The amount of relative wavelength shift due to the heating laser is dependent on both the wind speed and the heating laser power. The large fluctuation in wavelength when the heating laser was on, especially at higher power levels, is believed to arise from the locally instable wind speed rather than the noise of the sensor, as stable signal was observed before heating light was turned on. For reliable comparison, the mean value over a period of time is calculated and used as the wavelength under a certain condition.

Relative wavelength shifts when the heating laser was turned from off to on for the same wind speed but different wind temperatures are shown in Fig. 5(b) (red and green curves). To show the effectiveness of the temperature compensation using relative wavelength shift, the difference in the absolute wavelength of the fringe valley when the power was on for the same conditions, which corresponds to the case without temperature compensation, is also shown in Fig. 5(b) (black and blue curves). Clearly, the relative wavelength shift gives a signal that is much less sensitive to temperature. Taking the results for the heating laser power of 50 mA as an example, without temperature compensation, a difference of 0.362 nm was obtained for the same wind speed of 2.7 m/s under these two different wind temperatures. However, the difference in the relative wavelength shifts under the two different wind temperatures was dramatically reduced to 0.078 nm. Note that the results still deviate from the theoretical predictions that the relative wavelength shift is independent of wind temperature; in other words, the difference in the relative wavelength shift should be 0 at the two temperatures. The deviation is more significant especially when the heating power is higher (70 mA vs. 60 and 50 mA) as shown in Fig. 4(c). We believe that the deviations are mainly from the changes in coupling ratio of the fiber-optic coupler used to direct the 635 nm heating laser to the sensor head at different temperatures. As the fiber-optic coupler, made from SMF-28, is designed for operation in 1550 nm wavelength window and the fiber becomes multimode at the wavelength of 635 nm, the coupling ratio is sensitive to temperature variations. As a verification for this, according to Eq. (9), the ratio of the relative wavelength shifts in response to different wind speeds of u_1 and u_2 (i.e. $\Delta\lambda_1 / \Delta\lambda_2$) at the same wind temperature is equal to $u_1^{-1/2} / u_2^{-1/2}$, independent of the heating laser power. The ratios calculated according to the experimental results are listed in Table 1. It can be seen that the ratios are close to each other, which is an indication that the heating laser power variations are responsible for the deviations.

Table 1. Ratio of the wavelength shift to wind speed of 4 m/s to that of 2.7 m/s at different wind temperatures and heating laser currents.

Wind Temperature	Ratio ($\Delta\lambda_1 / \Delta\lambda_2$)		
	50 mA	60 mA	70 mA
19.7 °C	0.898	0.886	0.853
23.7 °C	0.891	0.887	0.850

Finally, we characterized the sensitivity and response time of the sensor to wind speed. The measured wavelength as a function of wind speed is shown in Fig. 6(a). It is clearly seen that the sensitivity is enhanced by increasing the heating power, consistent with Eq. (9). To examine the speed of the proposed anemometer, the sensor response upon turning on the wind tunnel is compared with that of the commercial anemometer in Fig. 6(b). The response time, defined as the time needed for 63% of the total signal change, is measured to be 0.14 s for the fiber-optic anemometer (see the inset to Fig. 6(b)), compared to 2.3 s for the commercial anemometer used in our experiment. Note that the response time measured here is limited to the speed of changes in the wind speed that can be obtained in the experiment. Fast response of the investigated fiber-optic anemometer is critical for the visualization of swift variation in local wind speed.

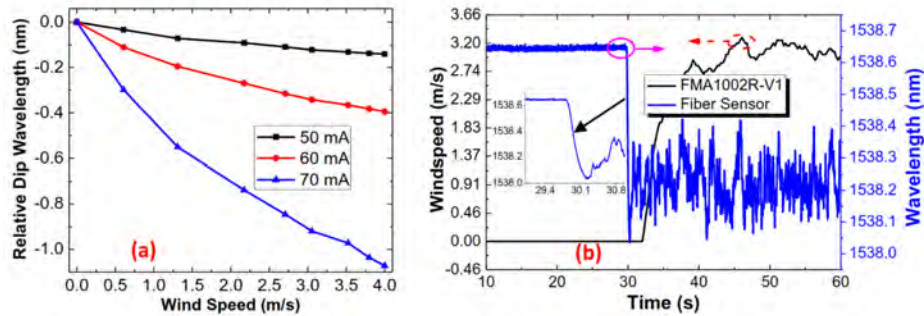


Fig. 6. (a) Relative dip wavelength versus wind speed at different heating laser currents. (b) Comparison of the responses between the fiber-optic sensor and the commercial FMA1002R-V1 anemometer when the wind is suddenly turned on. Inset to (b) is the enlarged view of the sensor response upon turning on the wind.

4. Conclusion

In summary, a novel fast-response fiber-optic anemometer based on a silicon FPI has been demonstrated and investigated. The silicon film is heated by a red diode laser while the signal light in the IR wavelength range is used to measure the temperature changes of the FPI with high speed. Due to cooling effects brought by wind, fringe valley wavelength of the reflection spectrum of the FPI experiences a blue shift. By measuring the wavelength difference when the heating laser is turned on and off, the wind speed is extracted with little sensitivity to temperature, which has been verified both theoretically and experimentally. Due to the large thermal diffusivity of silicon and the small sensor size, the proposed anemometer features a very fast response to the wind speed.

Acknowledgments

This work was partially supported U.S. Naval Research Laboratory under contract no. N0017315P0376 and U.S. Office of Naval Research under grant no. N000141310159. We thank Prof. Zhaoyan Zhang for stimulating discussions on the heat-transfer problem and Mr. Dustin Dam for technical support on the high-speed spectrometer.